Review article

M.A. Khan* and Michael N. Leuenberger*

Optoelectronics with single layer group-VIB transition metal dichalcogenides

https://doi.org/10.1515/nanoph-2018-0041
Received April 8, 2018; revised August 4, 2018; accepted August 6, 2018

Abstract: The discovery of two-dimensional (2D) materials has opened up new frontiers and challenges for exploring fundamental research. Recently, single-layer (SL) transition metal dichalcogenides (TMDCs) have emerged as candidate materials for electronic and optoelectronic applications. In contrast to graphene, SL TMDCs have sizable band gaps that change from indirect to direct in SLs, which is useful in making thinner and more efficient electronic devices, such as transistors, photodetectors, and electroluminescent devices. In addition, SL TMDCs show strong spin-orbit coupling effects at the valence band edges, giving rise to the observation of valley-selective optical excitations. Here, we review the basic electronic and optical properties of pure and defected group-VIB SL TMDCs, with emphasis on the strong excitonic effects and their prospect for future optoelectronic devices.

Keywords: 2D materials; transition metal dichalcogenides; defects; optoelectronics.

1 Introduction

Atomically thin materials have attracted a great deal of attention since they exhibit rich and intriguing properties that have been impossible to extract from their bulk counterparts. A typical layered material consists of a stack of planes of atoms held together through strong in-plane covalent and weak out-of-plane van der Waals forces [1]. The weak out-of-plane van der Waals forces enable the separation and isolation of stable atomically thin layers, the so-called 2D materials. An important property of 2D materials is their large surface-to-volume ratio that makes them very sensitive to external perturbations. It has been shown that the band gap in atomically thin materials can be tuned by changing the number of layers [2, 3] or as a function of strain [4], a property that is highly desirable in modern-day electronics industry. Secondly, the Fermi level and the charge density can be tuned as a function of external gate voltage, which enables the strong modulation of the electrical and optical properties of SL materials. Also, it has been shown that the charge density in doped 2D semiconductors is more stable against thermal fluctuations [5].

Graphene, a zero band gap semimetal, was the first 2D material that has been mechanically exfoliated [6] and is one of the most extensively studied 2D materials due to its wide range of promising applications in science and technology. However, graphene is not the best material for every application since its zero band gap hinders its application in high-performance field effect transistors and in optoelectronics. Soon after the discovery of graphene, the search for other 2D materials began, leading to the discovery of a slew of 2D materials [7, 8], such as hexagonal boron nitride, phosphorene, and single-layer (SL) transition metal dichalcogenides (TMDCs). TMDCs have the chemical composition of MX_2; M = transition metal such as Mo, W, Nb, Ta, Re, Zr, and X = S, Se, Te. They exhibit a wide range of properties. For example, NbS_2, $NbSe_2$, TaS_2, and $TaSe_2$ are metals in bulk form [9, 10], while ReS_2, $ReSe_2$, MoS_2, $MoSe_2$, WS_2, WSe_2, $MoTe_2$, and WTe_2 are semiconductors [11–15]. Among the various SL TMDCs, group-VIB ones (M=Mo, W; X=S, Se) have been most extensively studied, because they are found to be stable in air at room temperature [16, 17]. Also, we are interested in the optoelectronic properties and SL group-VIB TMDCs show excellent photoabsorption in the visible and near-infrared regions. Therefore, in this short review, we limit ourselves to group-VIB TMDCs such as MoS_2, $MoSe_2$, WS_2, and WSe_2

***Corresponding authors: M.A. Khan,** NanoScience Technology Center, University of Central Florida, Orlando, FL 32826, USA; Department of Physics, University of Central Florida, Orlando, FL 32816, USA; and Department of Applied Physics, Federal Urdu University of Arts, Science and Technology, Islamabad, Pakistan, e-mail: mahtab_afrasayab@knights.ucf.edu; and
Michael N. Leuenberger, NanoScience Technology Center, University of Central Florida, Orlando, FL 32826, USA; and Department of Physics, University of Central Florida, Orlando, FL 32816, USA, e-mail: michael.leuenberger@ucf.edu. http://orcid.org/0000-0002-7213-5866

and hereafter, the term TMDCs is specific for group-VIB TMDCs unless stated otherwise.

SL TMDCs are direct band gap semiconductors [3, 12] exhibiting a relatively high absorption in the visible and the near-infrared regions, which makes them ideal candidates for atomically thin photo-active materials [1, 18, 19]. Also, in contrast to graphene, SL TMDCs exhibit large intrinsic spin-orbit coupling (SOC) [13, 14], originating from the d-orbitals of the transition-metal atoms. Moreover, transport measurements such as on/off current ratio (up to 1×10^8) and steep subthreshold swing of 70 $mVdec^{-1}$ [20, 21] are clearly observed in TMDCs. All these fascinating properties make SL TMDCs promising candidate materials for nanoelectronic, optoelectronic, and spintronic devices.

Large-scale synthesis of 2D materials is one of the significant issues for fabricating practical devices made of layered materials. Different fabrication techniques such as chemical vapor deposition (CVD), physical vapor deposition (PVD), and molecular beam epitaxy (MBE) have been employed to obtain microscale samples. It has been observed that samples obtained through these techniques are highly poly-crystalline and include interfaces such as edges, heterostructures, grain boundaries, and most importantly point defects. These imperfections do not always degrade the materials properties, but they often bring new physics and even useful functionality.

Defects play an important role in tailoring electronic and optical properties of semiconductors and have been the subject of intense research over the last few decades. Point defects in semiconductors can trap charge carriers and localize excitons. Excitons bound to defects, if recombining radiatively, lead to light emission at lower energies than the optical interband transition. The interaction between these defects and charge carriers becomes stronger at reduced dimensionalities, which can be understood in a simplified hydrogenic model of excitons; for example, in three dimensions, shallow defects bind electrons at ground state binding energy equal to $13.6\ \mathrm{eV}\times m^*/\varepsilon_r^2$, where m^* and ε_r are effective mass and relative dielectric constant. This value increases to $54.4\ \mathrm{eV}\times m^*/\varepsilon_r^2$ [22] in 2D, simply due to the reduced dimensionality. Recently, in SL WSe_2, the exciton binding energy has been determined to be 0.37 eV, which is about an order of magnitude larger than the one observed in III–V semiconductor quantum wells, and therefore renders the exciton excited states observable even at room temperature [23].

In this short review, we first present electronic and optical properties of SL TMDCs. Then we present a survey of the hitherto reported point defects in SL TMDCs. This includes point defects, line defects, and heterostructures of different SL TMDCs. We will discuss the formation of defects and their influence on the electronic and optical properties of SL TMDCs. We will then briefly review recent progress in optoelectronics and photonics applications of defected TMDCs. Finally, we will discuss the major challenges and future opportunities in this rapidly progressing field of research.

2 Basic electronic structure and optical selection rules

Bulk TMDCs consist of stacked monolayers (MX_2) of atoms which are bonded through out-of-plane weak van der Waals forces, while each monolayer also has three stacked layers (X-M-X) of atoms held together through strong covalent bonds (Figure 1A). Bulk TMDCs have indirect band gaps (Γ and Q-points), lying below the direct gap by 0.6 eV (K and K′-point) in the case of MoS_2 (Figure 1B). However, as the number of layers decreases, strong confinement in the out-of-plane direction leads to a significant increase in the indirect gap while leaving the direct gap unaffected at the K(K′)-point (Figure 1B). This leads to a crossover to a direct-gap material in the limit of SL TMDCs. Thus, band gap engineering can be carried out by changing the number of layers in a given TMDC (Figure 1C).

The electronic states of a crystal transform according to the irreducible representations of the symmetry group of the crystal. SL TMDCs have D_{3h} point group symmetry. σ_h represents the reflection about the horizontal plane, passing through the origin and perpendicular to the axis with the highest symmetry, and is a symmetry operation of D_{3h}. SL TMDCs are invariant with respect to the σ_h reflection about the $z=0$ or M-plane of atoms, where the z-axis is oriented perpendicular to the M-plane of atoms. Therefore, electronic states break down into even and odd or symmetric and antisymmetric states with respect to σ_h. This leads to the nontrivial consequence that TMDCs have two band gaps, an in-plane $\varepsilon_{\|}$ and a substantially larger out-of-plane band gap $\varepsilon_{\perp}$ [24, 25]. The out-of-plane band gap $\varepsilon_{\perp}$ is a consequence of the nonzero thickness of SL TMDCs, which is usually neglected due to its substantially larger values for pristine cases. In TMDCs, d-orbitals of transition metal atoms and p-orbitals of chalcogen atoms contribute in the bonding process. From the first principle calculations, it has been shown that at band edges, contribution of the p-orbitals of the chalcogen atoms is small and the electronic structures of SL TMDCs near the band edges can be explained by considering the d-orbitals of the M atoms only [3, 9, 12, 26], especially d_{xy}, $d_{x^2-y^2}$, and

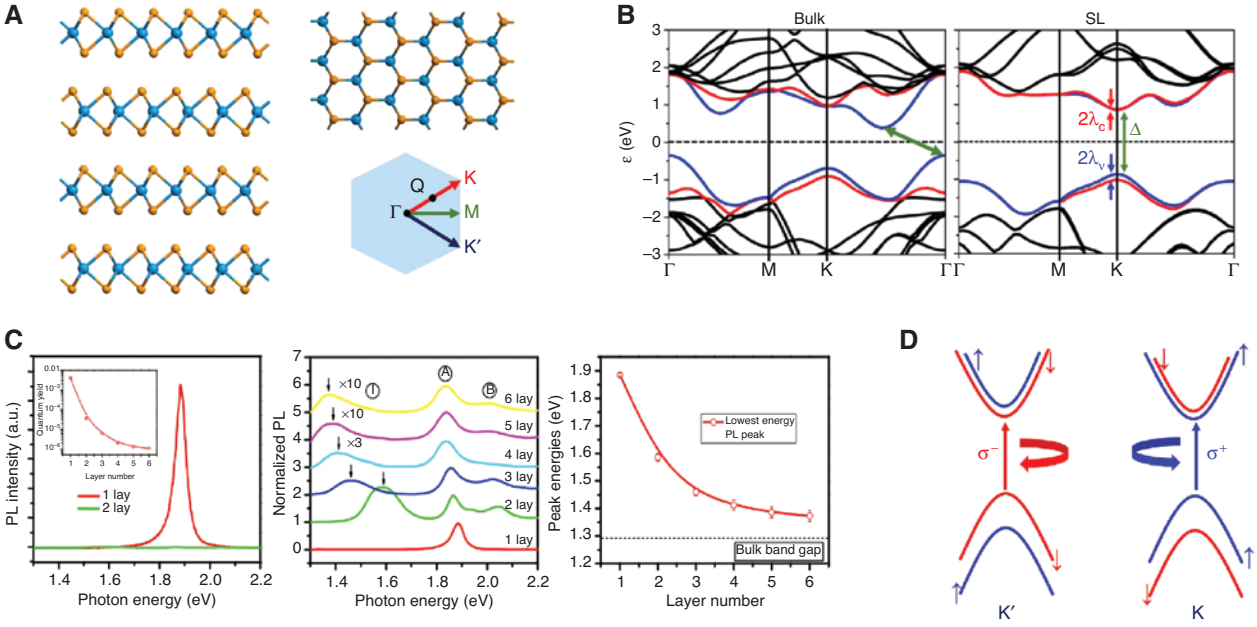

Figure 1: Electronic and optical properties of SL TMDCs.
(A) Structure of MX_2, blue spheres represents transition metal M atoms, while brown spheres represent chalcogen X atoms. (B) The energy band structure of bulk (left) and SL (right) pristine MoS_2, which shows that bulk MoS_2 is an indirect while SL MoS_2 is a direct band gap semiconductor. Basic topology of the band structure for all TMDCs is essentially the same, details are, however, different which are summarized in Table. 1. Blue curves show the valance band (VB) and conduction band (CB), while red curves show VB-1 and CB + 1. (C) Photoluminescence spectra, which show an order of magnitude difference in absorption between SL and bilayer MoS_2 [3]. Also it can be seen that band gap shifts as a function of thickness. (D) A schematic illustration of circular dichroism. Electronic bands around K and K′ points (for instance for MoX_2). Spin and valley degrees of freedom are locked together, which results in optical valley-dependent selection rules.

d_{z^2}. In the Brillouin zone, the Γ-point has the highest symmetry and is described by the D_{3h} point group, while the K and K′-points have lower symmetry and are described by C_{3h} point group. By using symmetry adopted basis, a 2-band k · p Hamiltonian [13] can be written as

$$\hat{H} = at(\tau\hat{\sigma}_x k_x + \hat{\sigma}_y k_y) + \frac{\Delta}{2}\hat{\sigma}_z - \lambda\tau\frac{\hat{\sigma}_z - 1}{2}\hat{s}_z, \qquad (1)$$

where a, t, σ_i's, and Δ are lattice constant, hopping integral, Pauli matrices, and band gap, respectively. These parameters are summarized in Table 1. $\tau = \pm 1$ is the valley index and $2\lambda_{v(c)}$ is the spin splitting at the valence (conduction) band edge due to the SOC. A similar Hamiltonian can also be derived by using the tight-binding model [27]. The orbital part of Hamiltonian Eq. (1) (first two terms) looks similar to the Hamiltonian of SL graphene with staggered sublattice potential, which is not surprising as both systems have essentially the same structural properties. The third term in Eq. (1) represents the SOC due to the broken inversion symmetry and due to the presence of heavy transition metal atoms (SOC ~ 150 (400) meV for Mo(W)X_2), in contrast to graphene (SOC ~ 1 meV), where SOC is strongly suppressed due to the inversion symmetry. Spin splitting in SL TMDCs at K and K′ points is opposite in sign due to time reversal symmetry. Therefore, the electromagnetic wave couples differently at the two valleys, i.e. right or left circularly polarized waves excite electrons in one of the valleys only, a phenomenon known as valley-dependent circular dichroism (CD) (Figure 1D). SL TMDCs provide an excellent platform to observe CD because of their hexagonal or honeycomb lattice structure, direct band gap, and large SOC. CD has been observed in MoS_2 [28–30]. An imbalance of charge carriers in the two valleys or valley polarization can be induced when charge carriers

Table 1: Fitting result from first-principles band structure calculations. The unit is Å for a, and eV for Δ, t, λ_v, λ_c.

	a	Δ	t	$2\lambda_v$	$2\lambda_c$
MoS_2	3.193	1.66	1.10	0.15	0.003
WS_2	3.197	1.79	1.37	0.43	−0.038
$MoSe_2$	3.313	1.47	0.94	0.18	0.023
WSe_2	3.310	1.60	1.19	0.46	−0.046

are excited by valley-selective CD. Valley polarization then leads to the so-called valley Hall effect, which has been observed for SL MoS_2 [31].

It should be noted that all bands are spin split due to the intrinsic SOC, except at the time reversal invariant points Γ and M. Smaller but significant spin splitting is also present at the conduction band edge due to the intrinsic SOC [32–34]. Interestingly, depending on the transition metal atom (Mo or W), the spin splittings at the conduction band edge have opposite signs; consequently, the lowest energy transitions in MoX_2 (WX_2) are made by bright (dark) excitons [35].

2.1 Excitons

As an SL material and due to weak electrostatic screening [27, 36, 37], TMDCs exhibit strong excitonic effects. An exciton is a bound state of an excited electron (in the conduction band) and a hole (electron vacancy in the valence band). The binding energy of an exciton in semiconductors can be understood in much the same way as the energy spectrum of a two-particle hydrogen model. For SL TMDCs, the simple 2D hydrogen model does not exactly reproduce the experimentally observed exciton binding energies, rather a modified 2D exciton model is required that essentially captures the effects of orbital and pseudospin angular momentum. Using Eq. (1), one may intuitively think that the energy spectrum of fully relativistic Dirac hydrogen atom may provide the solution, where the intrinsic spin arises inherently. However, the lack of agreement between the Dirac hydrogen spectrum and observed excitonic energies for SL TMDCs suggest that the pseudospin should be treated differently than the intrinsic spin of electrons. Starting from Eq. (1), the excitation spectrum for the experimentally relevant regime $\Delta \gg \varepsilon_b$ can be written as [38]

$$\varepsilon_{nj} = \Delta - \frac{e^4 \mu}{2\epsilon^2 \hbar^2 (n + |j| + 1/2)^2}, \tag{2}$$

where $j = m + 1/2$ is the total angular momentum, i.e. orbital m and pseudospin angular momentum 1/2. μ is the reduced mass of electron and hole, i.e. $\mu^{-1} = m_e^{-1} + m_h^{-1}$. By setting $j = m$ or ignoring the effect of pseudospin, Eq. (2) reduces to the energy spectrum of the 2D hydrogen atom. It should be noted that excitons in SL TMDCs retain the effects of both Dirac and Schrödinger quasiparticles. Eq. (2) shows good agreement with experimentally observed results [23, 39].

The crystal symmetry of the honeycomb lattice, the strong SOC, and the orbital character at the band edges in SL TMDCs lead to distinct excitonic flavors, such as bright excitons at the K and K′ points in the Brillouin zone, intravalley excitons with nonzero center-of-mass momentum, and inter- and intravalley dark excitonic states [27]. An excitation from valence to conduction band has to follow certain selection rules; a bright (dark) exciton is the bound electron and hole states which can recombine radiatively (nonradiatively) or which is allowed (forbidden) by certain optical selection rules. Dark excitons are generated as a result of complex scattering mechanisms, such as electric injection or electron–phonon interaction. The relative position of dark excitons with respect to optically accessible bright excitons plays a crucial role in determining the optical efficiency of a material. Several studies have been done to investigate the effects of dark excitons on the photoluminescence (PL) response of SL TMDCs [40–42]. In particular, it has been suggested that low PL intensity is not necessarily an indication of an indirect band gap, rather it can be ascribed to the relative spectral distance between dark and bright exciton states in SL TMDCs [42]. In another study, the life time of the dark exciton states in SL TMDCs has been found to be two orders of magnitude larger than the lifetime of the bright excitons at low temperatures [41].

For an optically allowed transition, the sum of the orbital angular momentum of the electronic states and the valley orbital angular momentum at the K or K' point should differ by one $-\tau_e$ [43]. In addition, the electron vacancy ($|v\rangle$) and hole ($|h\rangle$) states are connected through time reversal operation, i.e. $|h\rangle = K|v\rangle$. Time reversal operation reverses the momentum $k_{h(e)}$, spin $s_{h(e)}$, and valley $\tau_{h(e)}$ indices. This naturally defines the excitation of an electron through given polarization. For SL TMDCs, if an electron is excited to the conduction band as a result of an absorption of a photon with in-plane momentum $\mathbf{q}_{||}$ with polarization σ_+ in $s_e = 1/2$ state and $\tau_e = 1$, conservation of total momentum dictates that the center of mass of the electron–hole pair will have a net momentum $K_{cm} = k_h + k_e$. Accordingly, the hole valley index, $\tau_h = -1$, and spin, $s_h = -1/2$, are formally opposite to those of the conduction band electrons. In a similar manner, the absorption of a σ_- photon results in the formation of the electron–hole pair with $\tau_e = -\tau_h = -1$, $s_e = -s_h = -1/2$ [35, 44].

3 Defects in TMDCs

One of the greatest challenges being faced today in commercializing atomically thin materials is how to produce high-quality samples, on a large scale at low cost, and in a

controllable manner. The quality of samples plays crucial role as the presence of irregularities or defects in the crystalline structure have an adverse effect on the electronic and optical properties. The most common and energetically favorable irregularities are point defects, most important of them are antisite defects (Figure 2A) and vacancies (Figure 2B) [45, 46]. Various fabrication techniques such as MBE, PVD, and CVD have been employed to obtain the micrometer or wafer scale samples of SL TMDCs. Although CVD and mechanical exfoliation (ME) have been the most successful fabrication techniques to generate samples with high quality of SL TMDCs, studies show that those samples have an abundance of point defects (Figure 2C, D), most importantly S vacancies in MoS_2 due to the lowest formation energy of these defects. In contrast to MoS_2, scanning tunneling microscope (STM) images show that defects in CVD-grown WSe_2 reside on W sites instead of selenium sites [47]. This shows that the Se vacancy is not the most favorable defect in CVD-grown WSe_2. In addition to the S vacancy, S_2 and Mo vacancies have also been observed in MoS_2 [45].

The presence of point defects degrades material properties that may result in reduced charge carrier mobility and in poor optical response. It has been observed that experimentally attainable samples of MoS_2 have considerably lower carrier mobilities in the 0.5–3 $cm^2 V^{-1} s^{-1}$ range [6] than the theoretically predicted value of 410 $cm^2 V^{-1} s^{-1}$ [20, 21]. It has recently been suggested that this discrepancy between the predicted and observed values of carrier mobility is due to the presence of impurities created during the growth process [48, 49]. Point defects can also affect the optical properties, resulting in an inhomogeneous contribution to line width and line shapes in the radiative emission spectrum. Defects break the translational symmetry of the crystalline structure. Thus, in principle, defect states can exist anywhere in the band structure, i.e. within the valence or conduction bands with regular electronic states or most importantly with in the band gap region. Within the dilute limit, localized defect states behave as trapping centers for charge carriers. Excitons bound to these defect states, if recombine radiatively leads to the light emission at the subband gap energies. An important factor characterizing the defect transition from band to band transition is the lifetime of excitons, which is inversely related to the width of the transition peak in the PL spectrum.

Although crystalline imperfections degrade materials properties, but often they can bring new physics and

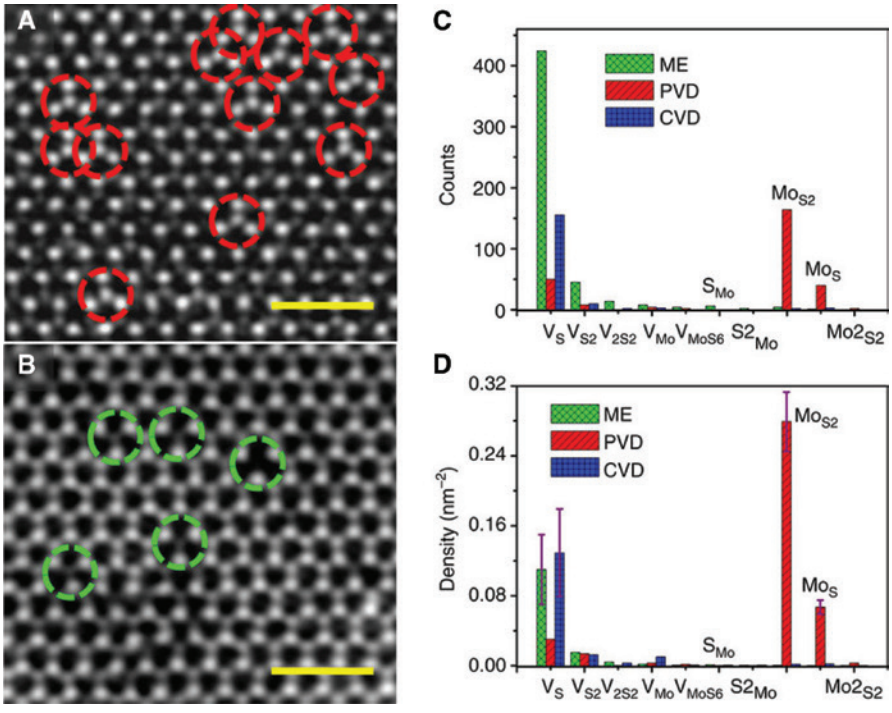

Figure 2: Growth related point defects, taken from Ref. [45].
(A) Antisite defects in PVD MoS_2 monolayer. Scale bar, 1 nm. (B) Vacancies including V_S and V_{S_2} observed in ME monlayers, similar to that observed for CVD sample. scale bar 1 nm. (C, D) Histogram of various point defects in PVD, CVD, and ME monolayers. ME data are in green, PVD data are in red, and CVD in blue.

even useful functionalities. Point defects are sometimes required and therefore can be created artificially, e.g. high-energy α-particle irradiation or by thermal annealing of SL TMDCs [50]. Photoluminescence measurements on the MoS_2 samples irradiated by high-energy α-particles show appearence of absorption peaks at subband gap frequencies. More importantly, an increase in the radiation dose, in the nitrogen-rich environment, leads to enhancement of PL intensity of both bound and free excitons.

It has been shown that oxygen irradiation of MoS_2 samples in the presence of S-vacancy leads to an enhancement of PL intensity as a function of exposure time (see Figure 3 [51]). The detailed structural analysis shows that an oxygen molecule (O_2) resides at the S-vacancy site in MoS_2. The adsorption of the oxygen molecule at the S-vacancy site exhibits strong bonding, introduces p-type doping in MoS_2, and hence a conversion from trion to exciton. Meanwhile, it has also been observed that the strong oxygen plasma treatment of mechanically exfoliated MoS_2 flakes can be used to tune the PL intensity from very high to complete quenching as a function of exposure time (see Figure 4). This behavior is a result of direct-to-indirect band transformation due to the formation of disordered regions made of MoO_3 in the MoS_2 flakes upon exposure to oxygen plasma [52].

Presence of certain vacancy defects such as S_2, Mo, and $3\times MoS_2$ leads to the sharp optical transition in the in-plane and out-of-plane component of the electric susceptibility [24, 25] in MoS_2 in the subband gap region. Specifically, even and odd characters (with respect to σ_h symmetry) of defect states play an important role in determining the in-plane or out-of-plane resonances in the susceptibility tensor [25]. Also, the odd states are essential to understand the out-of-plane optical transitions. It should be noted that odd states are usually neglected for pristine cases.

In addition to point defects, each exfoliated sample naturally has an edge, which breaks the periodicity of the crystalline structure. The chemical properties of edges are very much different from the internal structure. Also the electronic properties are very sensitive to the type of edges, i.e. armchair (AC) and zigzag (ZZ). DFT calculations show that MoS_2 nanoribbon with an AC edge has a very small band gap of 0.56eV, which can be further increased to 0.67eV with hydrogen adsorption [53]. These values are an order of magnitude smaller than the band gap 1.9 eV of MoS_2. An armchair edge has never been found experimentally, instead ZZ edges are always observed for TMDCs because of their considerably low formation energy [54, 55]. Theoretical calculations show that an MoS_2 nanoribbon with ZZ edge is always metallic [53, 56], which is contrary to the experimental findings, which shows strong photoluminescence absorption near the edge of the TMDC flake [51]. Later, it has been explained that oxygen adsorption at the (Mo) ZZ edges, along with complex reconstructions, can lead to a band opening of 1.27eV [57].

Recently, there has been a growing interest [58, 59] in the fabrication of in-plane and out-of-plane or lateral

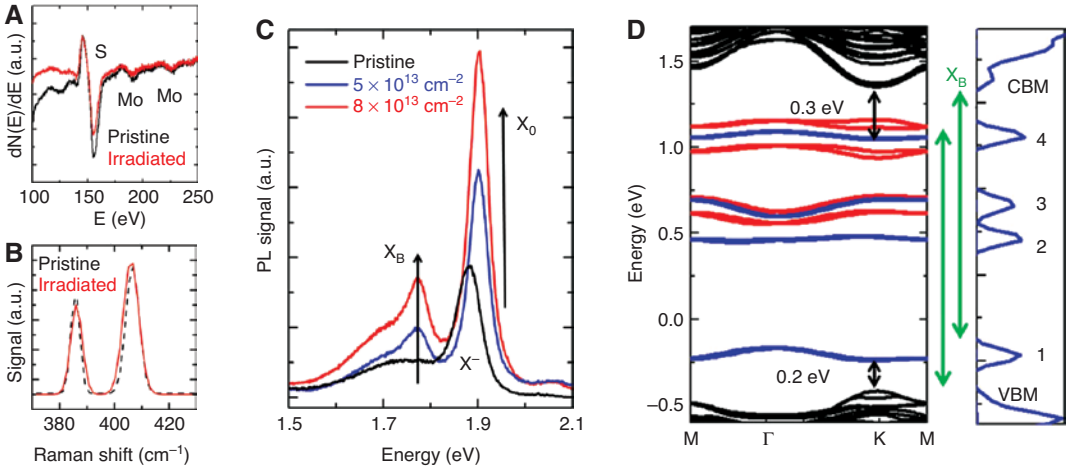

Figure 3: Defect-activated photoluminescence, taken from Ref. [50].
(A) Nano-Auger spectrum taken on MoS_2 before and after irrediation with α particles at dose 8×10^{13} cm^{-2}. (B) Raman spectrum of the same. (C) PL spectrum for pristine and irradiated monolayers MoS_2 at shown irradiation doses. The PL was taken at 77 K in N_2 (50 Torr) environment with a constant laser excitation power. The irradiation-caused enhancement in bound exciton (X_B) and free exciton (X_0) emission intensity are indicated. (D) Calculated band structure of monolayer MoS_2 in the presence of di-S vacancies. Red levels with in the band gap are levels appearing when S vacancies are introduced. Blue levels appear when N_2 molecules interact with S vacancies. Right panel: Total density of states of the monolayer MoS_2 with S vacancies in the poresence of N_2. Here the modeled vacancy density is 7×10^{13} cm^{-2}.

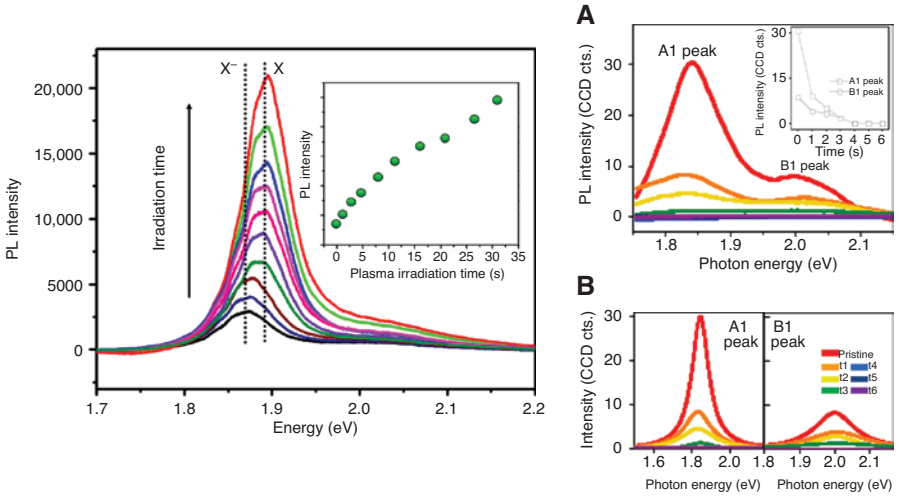

Figure 4: Photoluminescence quenching, taken from Ref. [51, 52].
Left, PL spectra of SL MoS_2 after oxygen plasma irradiation with different durations. The change of PL intensities with plasma irradiation times is shown in the inset. (Right, (A)) Time-dependent photoluminescence (PL) spectra of plasma-treated SL MoS_2. Inset shows the PL intensity of A_1 and B_1 peaks (corresponding to SOC) with respect to the plasma exposure time from pristine SL MoS_2 (red curve) to t_6 (purple curve). (B) Corresponding to A_1 and B_1 excitons, the peaks in PL spectra were fitted with Lorentzian functions.

and vertical heterostructures of different SL TMDCs. SL TMDCs are free of dangling bonds; therefore, they can be stacked vertically to form vertical heterostructure, which are bonded through van der Waal's interaction. Optical properties of few layer TMDCs are substantially different from the SL TMDCs; therefore, vertical heterostructure can be considered as a planar defect, which brings new opportunities for tuning the optical properties of the SL TMDCs. In Ref. [58], realization of one such heterostructure MoS_2/WSe_2 has been reported. The PL measurements show that the resultant bilayer MoS_2/WSe_2 system has a band gap of 1.50 eV, lower than the band gap energy of

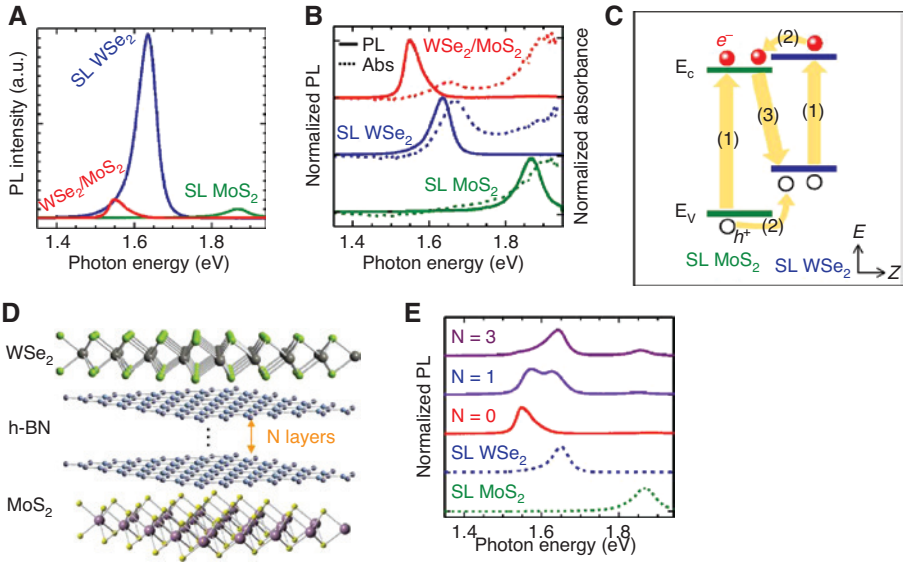

Figure 5: Photoluminescence and absorption from WSe_2/MoS_2 heterobilayers, taken from Ref. [58].
(A) PL spectra of single-layer WSe_2, MoS_2, and the corresponding heterobilayer. (B) Normalized PL (solid lines) and absorbance (dashed lines) spectra of single-layer WSe_2, MoS_2, and the corresponding heterobilayer, where the spectra are normalized to the height of the strongest PL/absorbance peak. (C) Band diagram of WSe_2/MoS_2 heterobilayer under photoexcitation, depicting (1) absorption and exciton generation in WSe_2 and MoS_2 single layers, (2) relaxation of excitons at the MoS_2/WSe_2 interface driven by the band offset, and (3) radiative recombination of spatially indirect excitons. (D) An atomistic illustration of the heterostructure of SL WSe_2/SL MoS2 with few-layer h-BN spacer in the vdW gap. (E) Normalized PL spectra from SL WSe_2/SL MoS2 heterostructure with n layers of hexagonal boron nitrite (n = 0, 1, and 3).

MoS_2 (~1.9 eV) and WSe_2 (~1.75 eV) (Figure 5). It should be noted that for vertical heterojuction, there is always an indirect transition due to the type-II band alignment. However, the PL intensity of the indirect transition is considerably strong, which shows the strong interlayer coupling of charge carriers. Controllable epitaxial growth enables the formation of seamless and sharp in-plane heterojunctions of two different SL TMDCs, such as MoS_2/WS_2 [59]. These heterojuctions are particularly interesting as the properties of these materials change drastically at the atomic level. The lateral heterostructure WS_2/MoS_2 shows photovoltaic effects under illumination due to the formation of a pn-junction in the SL materials in the absence of external gating. Strong and localized PL enhancement has been observed at the lateral interfaces due to the strong built-in electric field originating from the type-II band alignment [59].

4 Optoelectronics with TMDCs

Optoelectronics deals with the emission and detection of photons in a controllable manner. Nanomaterials such as carbon nanotubes and semiconductor quantum dots have been studied for the use in optoelectronic applications such as solar cells, lasers, LEDs, and photodetectors. Optoelectronic devices that are made of transparent materials are gaining immense interest due to their use in solar cells and transparent displays. The electronic band structure of materials is directly related to the absorption or emission of light. Graphene, the first 2D material, is a semimetal and is therefore not a suitable material to absorb light in the pristine form. Certain experimental techniques are devised such as doping and graphene patterning or chemical treatment [60, 61] to induce band gaps and enhance the optical response of graphene, which is necessary for optoelectronic applications. However, all these approaches require complex engineering, which is sometimes hard to accomplish.

In contrast to graphene, SL TMDCs are intrinsically direct band gap semiconductors and therefore provide a more straightforward platform for the realization of optoelectronic devices. SL TMDCs exhibit strong light–matter interaction [62, 63], arising from the band nesting and van Hove singularities in the density of states, in turn resulting in considerable absorption of light. Several studies show that TMDCs absorb 5–10% of the incident light, which is an order of magnitude higher than the conventional 3D semiconductors such as GaAs and Si. Furthermore, strong exciton and trion binding energies which are even visible at room temperature make them promising for the fabrication of high-performance atomically thin optoelectronic devices. The low dimensionality of 2D semiconductors makes them easily tunable, as the electrical, optical, and mechanical properties can all be controlled using multiple modulation methods. Such flexibility offers the potential for device applications such as tunable excitonic optoelectronic devices. The atomically thin van der Waal nature provides a platform for reducing the form factor and substrate-free assembly, compared to semiconductors requiring epitaxial substrates.

4.1 Light-mitting diodes (LEDs)

In LEDs, electrons and holes across a pn-junction recombine radiatively. The efficiency of an LED depends on the radiative recombination rate as there can be nonradiative pathways as well such as Auger recombination. SL materials-based LEDs have advantages over the conventional 3D semiconductor-based LEDs, given that the quantum efficiency of LEDs can be enhanced by avoiding the total internal reflections. An SL TMDCs-based atomically thin LED has been realized in vertical hetrojunction of p-type SL WSe_2 and n-type SL MoS_2. In contrast to conventional LEDs, light emission is not just confined to lateral hetrojuctions, but fast photoresponse is observed throughout the entire WSe_2/MoS_2 overlapping region. However, charge transfer takes place due to the type-II confinement at the vertical interface, which leads to the low quantum efficiency [64]. Also, the indirect band gap formation due to the mismatch of conduction electrons (n-type MoS_2) and valence band holes (p-type WSe_2) leads to low quantum yield of radiative recombination [64]. To enhance the quantum efficiency of SL TMDCs-based LEDs, a band engineering scheme has been devised such that the charge carriers remain confined within the emitting layer. A schematic diagram is shown in Figure 6, consisting of a stack of SL materials. Graphene layers are used for injecting holes and electrons [65]. The injected electrons and holes have to overcome the potential barrier given by hexgonal boron nitrite to reach to an SL of TMDC. This multiple quantum well device has an efficiency of 10%, which is comparable to the efficiency of modern-day organic LEDs [65, 66].

4.2 Photodetection

As a promising optoelectronic material, SL TMDCs can be used as semiconductor channel material in phototransistors, where light is converted directly into

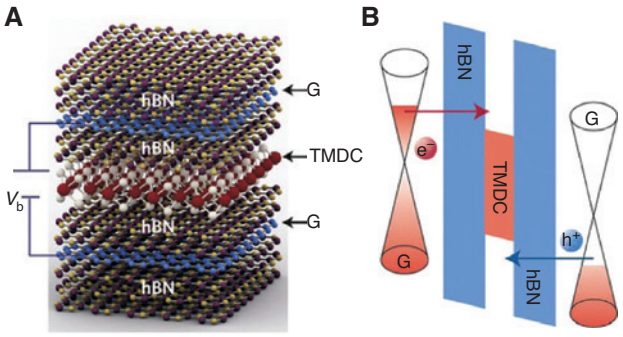

Figure 6: Van der Waals light-emitting diodes, taken from Ref. [62]. Schematic of a van der Waal's heterostructure operating as an LED. When a bias voltage V_b is applied to the graphene (G) electrodes, the injected charges recombine radiatively in the monolayer TMDC. (B) Band diagram of the LED with an applied bias. Electrons (e^-) and holes (h^+) from the graphene electrodes tunnel through the hexagonal Boron Nitrite dielectric layers (red and blue arrows) and reach the monolayer TMDC.

electrical current. The first MoS_2-based photodetector was reported in 2011 [67], which has has a photoresponsivity of 7.5 mAW^{-1}, comparable to the photoresponsivity of graphene-based devices. The main factor that hampers the performance of such a device is the need to generate a pn-juction that can separate the electron–hole pairs created by photon absorption. This problem has been solved by sandwiching the MoS_2 or WS_2 layer between layers of graphene, i.e. Gr/TMDC/Gr heterostructure. Graphene has a very high mobility, whereas SL TMDCs have high optical absorptions. It has been shown that Gr/TMDC/Gr-based phototransistors can show a photoresponsivity of 0.1 AW^{-1} [62]. Later, realization of an ultrasensitive SL MoS_2 photodetector has been demonstrated with an very high photoresponsivity of 880 AW^{-1} [68]. Such a high responsivity is a consequence of quality samples which show better mobility, clean contacts, and accurate positioning techniques of the contacts to collect the charge carriers.

5 Single quantum emitters

Single photon emission lies at the heart of many applications in photonics, including optical quantum computing [69] and quantum cryptography [70–72]. To make these

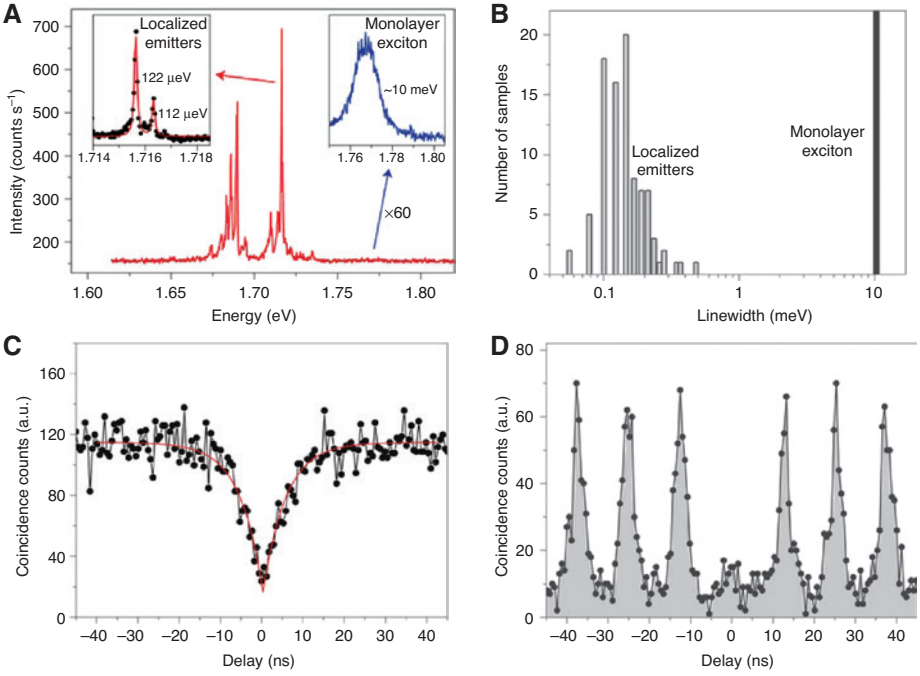

Figure 7: Emergence of narrow spectral lines and observation of photon antibunching, taken from Ref. [75].
(A) PL spectrum of localized emitters. The left inset is a high-resolution spectrum of the highest intensity peak (single quantum emitter). The right inset is a zoom-in of the SL valley exciton emission, integrated for 60 seconds. The emission of the localized emitters exhibits a red shift and much sharper spectral lines. (B) A histogram comparison of the linewidth between the emission from the delocalized valley exciton and 92 localized emitters, grouped in 23.3 μeV bins. (C) Second-order correlation measurement of the PL from SQE under a 6.8 μW CW laser excitation at 637 nm. The red line is a fit to the data, from which we extract $g^2(0) = 0.14 \pm 0.04$. (D) Intensity correlation measurement under 9.5 μW (average) pulsed excitation at 696.3 nm with a repetition rate of 82 MHz, and a pulse width of ~3 ps, which revealed $g^2(0) = 0.21 \pm 0.06$.

applications practical, solid-state single photon sources (SPSs) which can generate well separated (in time) and indistinguishable photons are required. Efforts have been made to develop single photon sources based on single molecules [73], quantum dots, and one-dimensional materials [74].

SPS based on SL WSe_2 have been reported recently in a series of publications [75–78]. It has been shown that long-lived localized exciton states bound to defects [75] or impurities [77] in SL WSe_2 decay radiatively, thereby emitting antibunched single photons at constant time intervals due to the Pauli exclusion principle Figure 7. In contrast to the free exciton emission, which has a broad line widths of (10 meV), the line width of the emitted single photons is very narrow (0.1 meV) (Figure 7B). The narrow line width of the emission spectra is a signature of the localized nature of the emission states. In a defect-free monolayer of WSe_2, light illumination creates delocalized excited states. However, the presence of defects in SL WSe_2 leads to localized excitonic states that can decay radiatively on a much slower rate, emitting one photon at a time. An atomically thin layer of WSe_2 has potential advantages over traditional solid-state emitters like nitrogen vacancy defects in diamond. For example, defects can exist naturally or can easily be introduced by irradiating the sample with a beam of high-energy particles. Photons from localized emitters in 3D materials have to travel through host media with a high refractive index, whereas in the case of a SL TMDC, photons can be immediately utilized with a strongly enhanced photon extraction efficiency. It may also be easier to integrate them into electronic devices than it is for other solid-state SPSs.

6 Outlook and conclusion

In this brief review, we present an overview of the basic electronic and optical properties of pure and defected SL TMDCs, with emphasis on their possible applications in future optoelectronic and photonic devices. SL TMDCs exhibit a number of exciting properties such as high optical response due to the direct band gap, band gap tunability, and strong SOC together with valley structure leading to circular dichroism, which are important both for fundamental research and for industrial applications. The presence of defects in SL TMDCs may lead to an enhancement of optical response at the subband gap energies, which are advantageous in making tunable light detectors. In addition, certain types of point defects in SL TMDCs enable the quantum emission of electrons at regular time intervals, giving rise to the single photon sources. Although new device concepts have shown the potential of SL TMDCs, many challenges have remained to be overcome and new opportunities are needed to be explored. Heterostructures of different SL TMDCs and with recently discovered atomically thin semiconductors such as phophorene [2, 4] provide new opportunities for band gap engineering to achieve desirable functionalities. However, there are certain challenges that should be met and overcome to fully appreciate the technological potential of SL TMDCs. One of the biggest challenges faced by the research community is the fabrication of high-quality, micrometer-sized samples of SL TMDCs to avoid the effects of grain boundaries. For solid-state samples, crystal growth methods need to be improved to achieve large areas, large grain sizes, uniformity, and control on the number of layers. The presence of defects significantly alters the materials' electronic and optical properties; however, it is encouraging that the effects of defects on SL TMDCs are not necessarily detrimental as long as it is possible to control the creation of the defects. At present, atomic scale synthesis and manipulation of defects remains a challenge. It is also a challenge for experimentalists to introduce specific types of defects into desired locations in controlled concentrations.

Acknowledgments: We acknowledge the support of NSF grant CCF-1514089.

References

[1] Bernardi M, Palummo M, Grossman JC. Extraordinary sunlight absorption and one nanometer thick photovoltaics using two-dimensional monolayer materials. Nano Lett 2013;13:3664–70.
[2] Cai Y, Zhang G, Zhang Y-W. Layer-dependent band alignment and work function of few-layer phosphorene. Sci Rep 2014;4:6677.
[3] Mak KF, Lee C, Hone J, Shan J, Heinz TF. Atomically Thin MoS_2: a new direct-gap semiconductor. Phys Rev Lett 2010;105:136805.
[4] Churchill HOH, Jarillo-Herrero P. Two-dimensional crystals: Phosphorus joins the family. Nat Nanotech 2014;9:330–1.
[5] Carvalho A, Neto AHC. Donor and acceptor levels in semiconducting transition-metal dichalcogenides. Phys Rev B 2014;89:081406.
[6] Novoselov KS, Jiang D, Schedin F, et al. Two-dimensional atomic crystals. Proc Natl Acad Sci USA 2005;102:10451–3.
[7] Mas-Balleste R, Gomez-Navarro C, Gomez-Herrero J, Zamora F. 2D materials: to graphene and beyond. Nanoscale 2011;3:20–30.
[8] Osada M, Sasaki T. Two-dimensional dielectric nanosheets: novel nanoelectronics from nanocrystal building blocks. Adv Mater 2012;24:210–28.
[9] Lebègue S, Eriksson O. Color rearrangements in B-meson decays. Phys Rev B 2009;79:115409.

[10] Ding Y, Wang Y, Ni J, Shi L, Shi S, Tang W. First principles study of structural, vibrational and electronic properties of graphene-like MX2 (M=Mo, Nb, W, Ta; X=S, Se, Te) monolayers. Physica B: Condensed Matter 2011;406:2254–60.
[11] Tongay S, Sahin H, Ko C, et al. Monolayer behaviour in bulk ReS2 due to electronic and vibrational decoupling. Nat Commun 2014;5:3252.
[12] Splendiani A, Sun L, Zhang Y, et al. Emerging photoluminescence in monolayer MoS2. Nano Lett 2010;10:1271–5.
[13] Xiao D, Liu G-B, Feng W, Xu X, Yao W. Coupled spin and valley physics in monolayers of MoS2 and other group-VI dichalcogenides. Phys Rev Lett 2012;108:196802.
[14] Liu G-B, Shan W-Y, Yao Y, Yao W, Xiao D. Three-band tight-binding model for monolayers of group-VIB transition metal dichalcogenides. Phys Rev B 2013;88:085433.
[15] Chuanhui G, Yuxi Z, Wei C, et al. Electronic and optoelectronic applications based on 2D novel anisotropic transition metal dichalcogenides. Adv Sci 2017;4:1700231.
[16] Geim AK, Grigorieva IV. Van der Waals heterostructures. Nature 2013;499:419–25.
[17] Liu G-B, Xiao D, Yao Y, Xu X, Yao W. Electronic structures and theoretical modelling of two-dimensional group-VIB transition metal dichalcogenides. Chem Soc Rev 2015;44:2643–63.
[18] Chao X, Chunhin M, Xiaoming T, Feng Y. Photodetectors based on two-dimensional layered materials beyond graphene. Adv Funct Mater 2016;27:1603886.
[19] Chuanhui G, Kai H, Xuepeng W, et al. 2D nanomaterial arrays for electronics and optoelectronics. Adv Funct Mater 2018;28:1706559.
[20] Radisavljevic B, Radenovic A, Brivio J, Giacometti V, Kis A. Single-layer MoS2 transistors. Nat Nanotechnol 2011;6:147–50.
[21] Fuhrer MS, Hone J. Measurement of mobility in dual-gated MoS2 transistors. Nat Nanotechnol 2013;8:146–7.
[22] Yang XL, Guo SH, Chan FT, Wong KW, Ching WY. Analytic solution of a two-dimensional hydrogen atom I Nonrelativistic theory. Phys Rev A 1991;43:1186–96.
[23] He K, Kumar N, Zhao L, et al. Tightly bound excitons in monolayer WSe2. Phys Rev Lett 2014;113:026803.
[24] Erementchouk M, Khan MA, Leuenberger MN. Optical signatures of states bound to vacancy defects in monolayer MoS2. Phys Rev B 2015;92:121401.
[25] Khan MA, Erementchouk M, Hendrickson J, Leuenberger MN. Electronic and optical properties of vacancy defects in single-layer transition metal dichalcogenides. Phys Rev B 2017;95:245435.
[26] Ataca C, Şahin H, Ciraci S. Stable, Single-layer MX2 transition-metal oxides and dichalcogenides in a honeycomb-like structure. J Phys Chem C 2012;116:8983.
[27] Berkelbach TC, Reichman DR. Optical and excitonic properties of atomically thin transition-metal dichalcogenides. Annu Rev Condens Matter Phys 2018;9:379–96.
[28] Zeng H, Dai J, Yao W, Xiao D, Cui X. Valley polarization in MoS2 monolayers by optical pumping. Nat Nanotechnol 2012;7:490–3.
[29] Mak KF, He K, Shan J, Heinz TF. Control of valley polarization in monolayer MoS2 by optical helicity. Nat Nanotechnol 2012;7:494–8.
[30] Cao T, Wang G, Han W, et al. Valley-selective circular dichroism of monolayer molybdenum disulphide. Nat Commun 2012;3:887.
[31] Mak KF, McGill KL, Park J, McEuen PL. The valley Hall effect in MoS2 transistors. Science 2014;344:1489–92.
[32] Kormányos A, Zólyomi V, Drummond ND, Rakyta P, Burkard G, Fal'ko VI. Monolayer MoS2: Trigonal warping, the Γ-valley, and spin-orbit coupling effects. Phys Rev B 2013;88:045416.
[33] Kormányos A, Burkard G, Gmitra M, et al. k · ptheory for two-dimensional transition metal dichalcogenide semiconductors. 2D Mater 2015;2:022001.
[34] Kormányos A, Zólyomi V, Drummond ND, Burkard G. Spin-orbit coupling, quantum dots, and qubits in monolayer transition metal dichalcogenides. Phys Rev X 2014;4:011034.
[35] Wang G, Chernikov A, Glazov MM, et al. Colloquium: excitons in atomically thin transition metal dichalcogenides. Rev Mod Phys 2018;90:021001.
[36] Qiu DY, da Jornada FH, Louie SG. Optical spectrum of MoS2: many-body effects and diversity of exciton states. Phys Rev Lett 2013;111:216805.
[37] Wu F, Qu F, MacDonald AH. Exciton band structure of monolayer MoS2. Phys Rev B 2015;91:075310.
[38] Trushin M, Goerbig MO, Belzig W. Optical absorption by Dirac excitons in single-layer transition-metal dichalcogenides. Phys Rev B 2016;94:041301.
[39] Chernikov A, Berkelbach TC, Hill HM, et al. Exciton binding energy and nonhydrogenic rydberg series in monolayer WS2. Phys Rev Lett 2014;113:076802.
[40] Echeverry JP, Urbaszek B, Amand T, Marie X, Gerber IC. Splitting between bright and dark excitons in transition metal dichalcogenide monolayers. Phys Rev B 2016;93:121107.
[41] Robert C, Amand T, Cadiz F, et al. Fine structure and lifetime of dark excitons in transition metal dichalcogenide monolayers. Phys Rev B 2017;96:155423.
[42] Malic E, Selig M, Feierabend M, et al. Dark excitons in transition metal dichalcogenides. Phys Rev Materials 2018;2:014002.
[43] Mak KF, Xiao D, Shan J. Light-valley interactions in 2D semiconductors. Nature Photonics 2018;12:451.
[44] Glazov MM, Amand T, Marie X, Lagarde D, Bouet L, Urbaszek B. Exciton fine structure and spin decoherence in monolayers of transition metal dichalcogenides. Phys Rev B 2014;89:201302.
[45] Hong J, Hu Z, Probert M, et al. Exploring atomic defects in molybdenum disulphide monolayers. Nature Comm 2015;6:6293.
[46] Zhou W, Zou X, Najmaei S, et al. Intrinsic structural defects in monolayer molybdenum disulfide. Nano Lett 2013;13:2615–22.
[47] Zhang S, Wang C-G, Li M-Y, et al. Defect structure of localized excitons in a WSe2 monolayer. Phys Rev Lett 2017;119:046101.
[48] Yu Z, Pan Y, Shen Y, et al. Towards intrinsic charge transport in monolayer molybdenum disulfide by defect and interface engineering. Nat Comm 2014;5:5290.
[49] Komsa H-P, Kotakoski J, Kurasch S, Lehtinen O, Kaiser U, Krasheninnikov AV. Two-dimensional transition metal dichalcogenides under electron irradiation: defect production and doping. Phys Rev Lett 2012;109:035503.
[50] Tongay S, Suh J, Ataca C, et al. Defects activated photoluminescence in two-dimensional semiconductors: interplay between bound, charged and free excitons. Sci Rep 2013;3:2657.
[51] Nan H, Wang Z, Wang W, et al. Strong photoluminescence enhancement of MoS2 through defect engineering and oxygen bonding. ACS Nano 2014;8:5738–45.
[52] Kang N, Paudel HP, Leuenberger MN, Tetard L, Khondaker SI. Photoluminescence quenching in single-layer MoS2 via oxygen plasma treatment. J Phys Chem C 2014;118:21258–63.

[53] Botello-Méndez AR, López-Urías F, Terrones M, Terrones H. Metallic and ferromagnetic edges in molybdenum disulfide nanoribbons. Nanotechnology 2009;20:325703.
[54] Wang Z, Li H, Liu Z, et al. Mixed low-dimensional nanomaterial: 2D ultranarrow MoS2 inorganic nanoribbons encapsulated in quasi-1D carbon nanotubes. J Am Chem Soc 2010;132:13840–7.
[55] Li Y, Zhou Z, Zhang S, Chen Z. MoS2 nanoribbons: high stability and unusual electronic and magnetic properties. J Am Chem Soc 2008;130:16739–44.
[56] Bertram N, Cordes J, Kim Y, Ganteför G, Gemming S, Seifert G. Nanoplatelets made from MoS2 and WS2. Chem Phys Lett 2006;418:36–9.
[57] Lucking MC, Bang J, Terrones H, Sun Y-Y, Zhang S. Multivalency-induced band gap opening at MoS2 edges. Chem Mater 2015;27:3326–31.
[58] Fang H, Battaglia C, Carraro C, et al. Strong interlayer coupling in van der Waals heterostructures built from single-layer chalcogenides. Proc Natl Acad Sci USA 2014;111:6198–202.
[59] Gong Y, Lin J, Wang X, et al. Vertical and in-plane heterostructures from WS 2/MoS 2 monolayers. Nat Mater 2014;13:1135–42.
[60] Eda G, Lin Y, Mattevi C, et al. Blue photoluminescence from chemically derived graphene oxide. Adv Mater 2009;22:505–9.
[61] Gokus T, Nair RR, Bonetti A, et al. Making graphene luminescent by oxygen plasma treatment. ACS Nano 2009;3:3963–8.
[62] Wang X, Xia F. Stacked 2D materials shed light. Nat Mater 2015;14:264–5.
[63] Carvalho A, Ribeiro RM, Castro Neto AH. Band nesting and the optical response of two-dimensional semiconducting transition metal dichalcogenides. Phys Rev B 2013;88:115205.
[64] Lee JY, Shin J-H, Lee G-H, Lee C-H. Two-dimensional semiconductor optoelectronics based on van der Waals heterostructures. Nanomaterials 2016;6:193.
[65] Withers O, Del Pozo-Zamudio F, Mishchenko A, et al. Light-emitting diodes by band-structure engineering in van der Waals heterostructures. Nat Mater 2015;14:301–6.
[66] Reineke S, Lindner F, Schwartz G, et al. White organic light-emitting diodes with fluorescent tube efficiency. Nature 2009;459:234–8.
[67] Yin Z, Li H, Li H, et al. Single-layer MoS2 phototransistors. ACS Nano 2012;6:74–80.
[68] Lopez-Sanchez O, Lembke D, Kayci M, Radenovic A, Kis A. Ultrasensitive photodetectors based on monolayer MoS2. Nat Nanotechnol 2013;8:497–501.
[69] Zadeh IE, Elshaari AW, Jöns KD, et al. Deterministic integration of single photon sources in silicon based photonic circuits. Nano Lett 2016;16:2289–94.
[70] Ekert AK. Quantum cryptography based on Bell's theorem. Phys Rev Lett 1991;67:661–3.
[71] Bennett CH, Wiesner SJ. Communication via one- and two-particle operators on Einstein-Podolsky-Rosen states. Phys Rev Lett 1992;69:2881–4.
[72] Bennett CH, Brassard G, Mermin ND. Quantum cryptography without Bell's theorem. Phys Rev Lett 1992;68:557–9.
[73] Moerner WE. Single-photon sources based on single molecules in solids. New J Phys 2004;6:88.
[74] Claudon J, Bleuse J, Malik NS, et al. A highly efficient single-photon source based on a quantum dot in a photonic nanowire. Nat Photonics 2010;4:174–7.
[75] He Y-M, Genevieve C, Schaibley RJ, et al. Single quantum emitters in monolayer semiconductors. Nat Nanotechnol 2015;10:497–502.
[76] Koperski M, Nogajewski K, Arora A, et al. Single photon emitters in exfoliated WSe2 structures. Nat Nanotechnol 2015;10:503–6.
[77] Srivastava A, Sidler M, Allain AV, Lembke DS, Kis A, Imamoğlu A. Optically active quantum dots in monolayer WSe2. Nat Nanotechnol 2015;10:491–6.
[78] Perebeinos V. Two dimensions and one photon. Nat Nanotechnol 2015;10:485–6.